

Protein stability engineering insights revealed by domain-wide comprehensive mutagenesis

Alex Nisthal^{1,4*}, Connie Y. Wang², Marie L. Ary² & Stephen L. Mayo^{1,3*}

¹Division of Biology and Biological Engineering, California Institute of Technology, Pasadena, CA 91125, USA. ²Protabit LLC, 1010 E. Union Street, Suite 110, Pasadena, CA 91106, USA. ³Division of Chemistry and Chemical Engineering, California Institute of Technology, Pasadena, CA 91125, USA. ⁴Present address: Xencor Inc., 111 W. Lemon Ave., Monrovia, CA 91016, USA. *Corresponding author

Abstract

The accurate prediction of protein stability upon sequence mutation is an important but unsolved challenge in protein engineering. Large mutational datasets are required to train computational predictors, but traditional methods for collecting stability data are either low-throughput or measure protein stability indirectly. Here, we develop an automated method to generate thermodynamic stability data for nearly every single mutant in a small 56-residue protein. Analysis reveals that most single mutants have a neutral effect on stability, mutational sensitivity is largely governed by residue burial, and unexpectedly, hydrophobics are the best tolerated amino acid type. Testing various stability prediction algorithms against our data shows that all perform moderately, and combinations of algorithms can better identify the most stable variants in the single mutant landscape. We find that strategies to extract stabilities from high-throughput fitness data such as deep mutational scanning are promising and may be applicable toward training future stability prediction tools.

Thermodynamic stability is a fundamental property of proteins that significantly influences protein structure, function, expression, and solubility. Efforts to identify the molecular determinants of protein stability and to engineer improvements have thus been crucial in the development and optimization of a wide range of biotechnology products, including industrial-grade enzymes, antibodies, and other protein-based therapeutics and reagents¹⁻³. The ability to reliably predict the effect of mutations on protein stability would greatly facilitate engineering efforts, and much research has been devoted to developing computational tools for this purpose⁴⁻⁹. Understanding how mutations affect stability can also shed light on various biological processes, including disease and drug resistance¹⁰. More than 100,000 genetic variants have been associated with human disease¹¹ thanks to recent advances in genotyping and next generation sequencing, demonstrating a large need for fast and accurate stability prediction.

However, the accurate prediction of the impact of an amino acid substitution on protein stability remains an unsolved challenge in protein engineering. Correlation studies have shown that computational techniques can capture general trends, but fail to precisely predict the magnitude of mutational effects^{12,13}. The success of these techniques is dependent on the quality of the input structure, conformational sampling, the free energy function used to evaluate the mutant sequences, and importantly, the data used for training and testing^{8,12,14}. Traditionally, protein stability data are collected by generating and purifying a small set of selected protein variants for characterization via calorimetry or spectroscopically measured chemical or thermal denaturation experiments. Values typically determined include the chemical or thermal denaturation

midpoint (C_m or T_m , respectively), the free energy of unfolding (ΔG), and the change in ΔG relative to wild type (WT) ($\Delta\Delta G$). Although low-throughput, the widespread use of these methods has generated a wealth of protein stability data over time, which has shaped our current understanding of protein structure-function relationships¹⁵⁻¹⁸. Much of this work has been aggregated in the ProTherm¹⁹ database, commonly used as a training data resource. Until recently, ProTherm was the largest public source of thermodynamic protein stability data, containing over 25,000 entries from 1,902 scientific articles. The database has been critical to the development of a variety of computational tools, from knowledge-based potentials exclusively trained on experimental data⁶ to physics-based potentials with atomic resolution⁷ and everything in between. Unfortunately, the ProTherm website is no longer being supported. The ProTherm data are still available, however, in ProtaBank²⁰, a recently developed online database for protein engineering data (<https://protabank.org>).

Although training and validation datasets from ProTherm have been widely used, ProTherm data suffer from three flaws: (1) experimental conditions vary widely among entries, requiring manual filtering to obtain comparable data, which results in smaller datasets, (2) little information is included on unfolded or alternatively folded sequences, precluding training on this type of mutational data, and (3) results from alanine scanning mutagenesis are overrepresented, biasing the dataset toward large to small mutations. Thus, training or testing on ProTherm data may mask deficiencies in computational algorithms or result in predictions that are biased toward particular features of the dataset. As many of the stability prediction tools available today rely on experimental

data from ProTherm, it is perhaps not surprising that none are very accurate and all perform about the same¹².

Comprehensive mutagenesis studies, with stabilities measured under fixed experimental conditions, could provide better training data. The low-throughput nature of traditional methods, however, makes the collection of stability data for large numbers of protein variants unfeasible. Several strategies have been devised to improve this process, including the use of genetic repressor systems²¹, plate-based fluorescence assays^{22,23}, differential scanning fluorimetry²⁴, and more recently, yeast-displayed proteolysis²⁵. Unfortunately, these approaches generally make compromises by either: (1) tying an easy-to-measure but indirect protein stability readout to large variant libraries, or (2) addressing the throughput of stability determination, but not the laborious nature of variant generation and purification.

Here, we develop an automated method that addresses both of these issues and apply it to obtain thermodynamic stability data from the comprehensive mutagenesis of an entire protein domain—the 56-residue β 1 domain of Streptococcal protein G ($G\beta$ 1). $G\beta$ 1 was chosen for its small size, high amount of secondary structure, and well-behaved WT sequence. Drawing both inspiration and methodology from structural genomics, we couple automated molecular biology procedures with a high-throughput plate-based stability determination method, resulting in a 20-fold increase in throughput over traditional bench-top methods. We applied our experimental pipeline to $G\beta$ 1 to produce a dataset that maintains constant experimental conditions, includes data on non-folded sequences, and features an unbiased mutational distribution over 935 unique variants covering nearly every single mutant of $G\beta$ 1. Data in hand, we examine

positional sensitivity and amino acid tolerance, and evaluate several protein stability prediction algorithms and engineering strategies. Finally, we compare our dataset against one derived by deep mutational scanning (DMS), a technique that can generate large mutational datasets via functional selections and deep sequencing^{26,27}, and explore whether stability data from DMS studies are applicable towards training future protein stability prediction tools.

Results

Automated site-directed mutagenesis and stability determination pipeline increases throughput 20-fold. Using laboratory automation, we constructed, expressed, and purified nearly every single mutant in G β 1. The automated pipeline is illustrated in Fig. 1a. Each variant was constructed explicitly instead of by saturation mutagenesis so that mutants not found in the first pass could be more easily recovered. Variants were constructed using a megaprimer method that requires only one mutagenic oligonucleotide, thereby halving oligonucleotide costs. The thermodynamic stabilities of the generated variants were then determined using an improved version of our previously described plate-based chemical denaturation assay²² (Fig. 1b). Enhancements include adaptation to automated liquid handling for increased speed and precision, and doubling the number of data points collected per curve to improve accuracy. Although the intent was to collect data on 19 amino acids at 56 positions for a total of 1,064 variants, a tradeoff was made in which mutations at the buried tryptophan (Trp) at position 43 (W43) were excluded to preserve the integrity of the Trp-based fluorescence assay. Also, mutations incorporating cysteine (Cys) or Trp were omitted to avoid oligomerization by disulfide formation and potential interference with W43,

respectively. Thus, mutations to 17 of 19 possible amino acids were made at 55 of 56 positions, for a total of 935 single mutants.

Each step of the workflow was developed as an independent module, allowing for optimization outside the full experimental pipeline. Modularization also permits flexible scheduling and parallelization, allowing modules to run multiple times per day. For comparison, eight days is a reasonable estimate for traditional procedures to construct, verify, express, purify, and measure the thermodynamic stability of 8 single mutants. Extrapolating to 935 variants (the number in this study), traditional procedures would take 935 days, or 2.5 years. In contrast, our platform can generate data on 935 variants in 5–6 weeks, a speedup of at least 20-fold.

Stability determination of Gβ1 single mutants. We measured the Trp fluorescence of each variant in response to a 24-point guanidinium chloride (GdmCl) gradient, thereby generating an unfolding curve (Fig. 1b) from which we determined the concentration of denaturant at the midpoint of the unfolding transition (C_m) and the slope (m -value)²⁸. While $\Delta\Delta G$ can be calculated in multiple ways (Supplementary Methods), a more precise method for our data takes the difference between the mutant and WT C_m values and multiplies it by their mean m -value (\bar{m})²⁹ as shown in the following equation:

$$\Delta\Delta G = \bar{m} \times (C_{m \text{ mutant}} - C_{m \text{ WT}})$$

where the m -value was obtained with the linear extrapolation method³⁰. Using this equation, stabilizing mutations have positive $\Delta\Delta G$ values, and destabilizing mutations have negative values. Of the 935 variants analyzed, 105 failed the assumptions of the linear extrapolation method (reversibility of folding/unfolding and two-state behavior) due to poor stability, presence of a folding intermediate, or no expression

(Supplementary Fig. 1). The 830 variants that passed these criteria are referred to as the quantitative dataset, and the remaining 105 are referred to as the qualitative dataset. The single mutant stabilities ($\Delta\Delta G$ s) for the entire dataset are shown as a heat map in Fig. 2.

Stability distribution of G β 1 single mutants is primarily neutral. The $\Delta\Delta G$ distribution of G β 1 single mutants is primarily neutral ($\Delta\Delta G$ of 0 ± 1 kcal/mol) with a long tail of destabilizing variants (Fig. 3a). The median of the quantitative dataset is 0.05 kcal/mol with an interquartile range of 1.0 kcal/mol (Fig. 3c), and the fraction of positive, neutral, and negative mutations is 3%, 68%, and 29%, respectively. If we assume the qualitative data contains only negative mutations, then our complete dataset shifts the fractions to 3%, 60%, and 37%, respectively. Summing the positive and neutral mutations, almost two thirds of the tested single mutants (63%) have at worst no effect on G β 1 stability. The fraction of destabilizing mutations (37%) is on the low end compared to an experimental dataset of 1285 mutants from ProTherm, which shows that ~50% of single mutants are destabilizing ($\Delta\Delta G < 1$ kcal/mol)^{31,32}. The destabilizing fraction we obtained for G β 1 would likely increase, however, upon making mutations to W43 and including Trp and Cys scanning variants as these residues are generally difficult to substitute in or out³³. Also, the G β 1 domain itself may skew mutational outcomes as its small size results in a large surface-to-buried area ratio. This ratio likely contributes to fewer destabilizing mutations than larger proteins with larger cores, assuming that most core mutations are destabilizing^{16,21,34,35}.

Positional sensitivity is governed by residue burial. The heat map in Figure 2, which is organized by primary structure, allows for a granular look at the distribution of mutational stability. We observe two clear trends: (1) the mutational sensitivity ($\Delta\Delta G$) of the domain is largely determined by the position of the mutation, not the amino acid identity, unless (2) the mutations are to glycine (Gly) or proline (Pro), for which most mutations are deleterious. Positions 3, 5, 26, 30, 41, 45, 52, and 54 are particularly sensitive to mutation. If we map the positional sensitivity (median $\Delta\Delta G$ at each position) onto the G β 1 structure (Fig. 4), we see that residues in the interior of the protein are more susceptible to destabilization. This is also observed when analyzing the distribution by tertiary structure, but not by secondary structure (Fig. 3c). That is, classifying residues into core, boundary, or surface with the RESCLASS algorithm⁴ shows that the median $\Delta\Delta G$ for core residues is ~ 1.5 kcal/mol lower than that of the rest of the protein. In addition, the qualitative dataset, which contains mutants whose stabilities are difficult to measure or are fully unfolded, has 5-fold more core variants as compared to the boundary or surface, adding further support to this observation (Fig. 3b). Although this relationship has been observed with other datasets using a variety of proxies for protein stability^{16,21,34,35}, this study provides a comprehensive analysis at the whole domain level with direct thermodynamic stability measurements.

As seen in Fig. 2, however, not all core positions behave the same, as some are more sensitive to mutation than others. For engineering purposes, it would be useful to identify specific protein attributes that could serve as quantitative predictors of positional sensitivity. We therefore performed linear regression with 10-fold cross validation on a large number of attributes that might impact protein stability. Attributes tested included

measures of residue burial, secondary structure type/propensity, structural flexibility, and the change upon mutation of residue descriptors such as hydrophobicity, volume, and charge. The best individual predictors were measures of residue burial: depth of the C β atom^{36,37} and occluded surface packing (OSP)^{38,39}, with correlation coefficients (r) of 0.82 and 0.76, respectively. This demonstrates that not all core positions are created equal, and that there is a direct relationship between how buried a position is and its sensitivity to mutation. Flexibility descriptors such as root mean squared fluctuations (RMSF) (from molecular dynamics simulations) or secondary structure descriptors such as α -helix propensity performed less well ($r = 0.42$ and 0.06 , respectively). We repeated these analyses with sequence entropy⁴⁰ as an alternative metric of positional sensitivity, and the conclusions remain the same (C β depth and OSP were the two best predictors, with $r = 0.81$ and 0.78 , respectively). Combinations of attributes were also tested, but these did not substantially improve predictability. Given the strong correlation between positional sensitivity and residue burial indicators like OSP and C β depth, calculation of these measures should be among the first tools employed when evaluating positions for substitution, provided structural information is available.

Hydrophobics are the best tolerated amino acid type. A common practice in protein redesign and optimization is to restrict core residues to nonpolar amino acids and only allow polar amino acids at the surface. We tested the validity of this strategy with our quantitative dataset by calculating median $\Delta\Delta G$ by incorporated amino acid and ranking the amino acids from worst tolerated to best tolerated across the entire domain (Fig. 5a). In general, the two worst amino acids for incorporation are Pro and Gly, which is unsurprising given their vastly different Ramachandran preferences compared to all

other amino acids. Beyond secondary structure-breaking amino acids, the third worst tolerated amino acid, interestingly, is aspartic acid (Asp), which may be rationalized by the fact that it is very hydrophilic⁴¹ and has one of the highest charge densities among the amino acids⁴². Unexpectedly, hydrophobic amino acids, particularly isoleucine (Ile) and phenylalanine (Phe), are among the best tolerated residues across all G β 1 positions. Even among surface positions, which make up over 50% of the dataset, Ile is the most favored individual residue, and hydrophobic amino acids as a whole are favored equally or better than the other amino acid types (Fig. 5b). The preference for hydrophobic amino acids extends to the chemically similar amino acid pairs, Asp/Glu and Asn/Gln, where the pair member containing the extra methylene is better tolerated across the domain (Fig. 5a) and in almost every RESCLASS environment (Fig. 5c). To determine if this observation is unique to G β 1, we performed domain-wide *in silico* stability predictions^{6,43} on five compositionally diverse proteins, including G β 1 (Supplementary Table 1). Remarkably, the calculations recapitulated our observations for G β 1 and produced similar results for the other proteins, even across different RESCLASS types (Supplementary Fig. 3).

Several other experimental studies have also found that hydrophobic amino acids are well tolerated on the surface⁴⁴⁻⁴⁸. The investigators attributed these findings to unique amino acid properties or structural contexts that enable these nonpolar mutations to stabilize the mutation site. However, our results suggest that non-position-specific increases in nonpolar surface area and volume are well tolerated, and the more the better. Larger hydrophobic amino acids like Ile, Phe, and Tyr are consistently ranked as the best tolerated, and smaller hydrophobics like Ala or Val do much worse across all

three residue classes, including surface residues (Fig. 5b). Although multiple nonpolar mutations to the surface are still likely deleterious to protein stability and solubility⁴⁵, single mutations to hydrophobic amino acids should not be categorically excluded for stability optimization.

Benchmarking protein stability prediction algorithms. We evaluated the ability of three stability prediction algorithms, PoPMuSiC⁴³, FoldX⁷, and Rosetta^{5,8}, to recapitulate the 830 $\Delta\Delta G$ values in our quantitative dataset. To better understand the effect of training data on each algorithm's performance, we compare the mutational composition of $\Delta\Delta G$ datasets used in the development of each algorithm (Table 1). PoPMuSiC is a simplified-representation statistical energy function trained on a very large experimental dataset from ProTherm. FoldX is similarly trained, albeit with a smaller and more Ala biased dataset, and mixes all-atom physical potentials with weighted statistical terms. Rosetta also mixes statistical and all-atom physical potentials, but is trained to recover native sequence compositions for protein design. A recent study systematically explored the effect of 19 different Rosetta parameter sets on single mutant stability prediction⁸, four of which are evaluated here. Three of the tested parameter sets use identical weights and terms but allow increasing amounts of backbone flexibility. That is, after sidechain repacking, the structure either undergoes no energy minimization, constrained backbone minimization, or unconstrained backbone minimization. Initially described as row 3, row 16, and row 19⁸, we refer to these parameter sets here as NoMin, SomeMin, and FullMin, respectively. The fourth Rosetta parameter set evaluated here (SomeMin_ddg) combines constrained minimization with optimized amino acid reference energies trained on single mutant $\Delta\Delta G$ data from ProTherm,

similar to FoldX and PoPMuSiC. Overall algorithm performance was evaluated by Pearson correlation coefficients (Table 2) and for both tertiary structure (RESCLASS) and volume change to assess performance by mutation type. As energies from physical potentials can be dramatically skewed by atomic clashes, we excluded mutations with exceptionally high clash energies (clash outliers).

The Rosetta SomeMin method is the best performing algorithm overall with a Pearson correlation coefficient of 0.64 (Table 2). The other methods perform less well at $r = 0.56$ (PoPMuSiC) and $r = 0.51$ (FoldX). All of the algorithms scored lower on our dataset than previously reported on independent test sets, where r values of 0.69 (Rosetta SomeMin)⁸, 0.67 (PopMuSiC)³⁷, and 0.64 (FoldX)⁴ were obtained. Comparing the different Rosetta methods, we observe that increasing backbone flexibility decreases the number of clash outliers, but does not necessarily improve overall performance. The constrained minimization in SomeMin considerably improves the correlation over NoMin, but unconstrained minimization in FullMin shows diminishing returns in allowing increased flexibility, as observed previously⁸. Significantly, the Rosetta SomeMin_ddg method performed worse than the SomeMin method ($r = 0.54$ and 0.64, respectively), demonstrating a limitation of training all-atom potentials with small, biased experimental datasets (Table 1).

If we look at the Pearson correlation coefficient by residue class, we find a general performance trend of boundary > surface > core. Except for Rosetta NoMin, which performs poorly across all categories, the all-atom algorithms exhibit very strong correlations in the boundary ($r \approx 0.7$), with weaker correlations on the surface ($r \approx 0.5$). In contrast, PoPMuSiC performs similarly across these two residue classes ($r = 0.56$

and $r = 0.51$, respectively). All algorithms do a poor job at predicting core mutations (r values range from 0.13 to 0.37), possibly because these mutations are more likely to lead to structural rearrangements that are not well captured by the algorithms⁶⁻⁸. The significant differences in correlation accuracy observed here likely do not stem from deficiencies in training data, as the composition by residue class is fairly uniform across algorithms (Table 1).

The data were also analyzed by mutations that either reduce side chain volume (large to small, $-Vol\Delta$) or increase side chain volume (small to large, $+Vol\Delta$). Overall, across all methods, large to small mutations are better predicted than the inverse, which correlates with the composition of the training sets used in algorithm development (Table 1).

All algorithms were also evaluated by the Spearman correlation coefficient to minimize penalties on skewed energies and instead reward correct rank ordering. The differences found with the Pearson method on the overall dataset are no longer observed (Supplementary Table 2). PoPMuSiC and all the Rosetta methods perform about the same, with FoldX performing less well. The performance trend between residue classes is retained with boundary > surface > core, and the performance edge for large to small mutations is widened when evaluated by the Spearman coefficient. Because mutations that remove substantial volume often create a destabilizing cavity⁴⁹, the direction of the stability change of large to small mutations is more easily predicted and indeed captured by all of the algorithms equally well. The small to large mutation type can have very different outcomes (stabilized backbone accommodation or under/over-packed destabilization) and thus is harder to rank, much less predict

accurately, as observed here. The volume change performance trend demonstrates why stability predictors often feature favorable correlation coefficients on test sets containing a bias towards mutations to small amino acids like Ala, which is nearly always overrepresented in the datasets, as observed in Table 1.

Practical stability engineering with *in silico* methods. As shown above and previously¹², highly accurate stability prediction ($r > 0.8$) is beyond current algorithms. However, this limitation has not prevented the successful application of *in silico* tools to stabilize proteins and engineer protein interaction specificity⁵⁰. One common approach is to: (1) generate stability predictions for every single mutant of a domain, (2) filter the stability predictions by an arbitrary $\Delta\Delta G(\text{predicted})$ cutoff, (3) experimentally verify the small number of mutants above the cutoff, and (4) combine the hits. Here, our objective is to identify the *in silico* method that best performs this task on our G β 1 dataset. That is, determine which algorithm recovers the greater number of stable variants (i.e., hits) near the top of its own predicted single-mutant list. We do this by calculating a couple of metrics across the two sorted lists of experimental and predicted variants, and, starting from the most stable variant, sequentially increase the number of mutants (N) that are compared. The first metric, % enrichment (% E), records the percent overlap between a list of experimentally verified mutants and a list of *in silico* predictions:

$$\%E(N) = \frac{\omega(N)}{N}$$

where $\omega(N)$ is the number of mutants found in both the experimental and predicted lists when N mutants are compared. The second metric, positive predictive value (PPV), first classifies the experimental dataset into “good” variants with $\Delta\Delta G > 0$ and “bad” variants

with $\Delta\Delta G \leq 0$, and then uses receiver operating characteristic (ROC) methods to calculate the fraction of true positives out of all positive predictions:

$$PPV(N) = \frac{TP(N)}{TP(N) + FP(N)}$$

where $TP(N)$ is the number of true positives when comparing lists of N mutations and $FP(N)$ is the number of false positives when comparing lists of N mutations. Although both methods focus on positive predictions, %E is more sensitive to how stability algorithms order their comprehensive single mutant predictions, whereas PPV will give a favorable score as long as the mutants predicted are classified as “good” ($\Delta\Delta G > 0$).

Values of %E and PPV as a function of the number of mutants (N) in the comparison, or $\%E(N)$ and $PPV(N)$, were calculated for FoldX, PoPMuSiC, and the four Rosetta methods. All the combinations of the *in silico* methods were also tested by taking the mean of the predictions and then calculating $\%E(N)$ and $PPV(N)$ as before. Focusing on the top 175 variants, which correspond to $\Delta\Delta G > 0.5$, both metrics indicate that Rosetta NoMin is the best single algorithm (Fig. 6 and Supplementary Fig. 4). If we limit N to the top 20 variants, such as if experimental throughput is limiting, the Rosetta methods with backbone flexibility outperform Rosetta NoMin. When considering combinations of algorithms, the best performers are PoPMuSiC with either Rosetta NoMin or Rosetta SomeMin (Fig. 6). These two combinations have a higher $\%E(N)$ and $PPV(N)$ than any single algorithm or any other combination of two algorithms when measuring the area under the curve (AUC). Nearly all three-algorithm combinations fail to outperform PoPMuSiC+Rosetta NoMin, indicating diminishing returns upon adding more algorithms. Prior work also indicates that combinations of algorithms outperform single algorithms in predicting the best single mutants^{45,50}. We found this to be true

across our entire dataset and with both metrics, except when FoldX is included in the combination (data not shown).

Note that the relationship between the number of variants and the $PPV(N)$ values depends on the stability distribution of the protein of interest. Not every protein domain will have more than 175 variants experimentally determined to have $\Delta\Delta G > 0$ to use in a “good” classification. In contrast, the $\%E(N)$ metric is independent of the stability distribution, and its values can be compared to prior studies using arbitrary $\Delta\Delta G$ cutoffs. Across nine studies using only FoldX and a $\Delta\Delta G$ cutoff, there were 81 true positives predicted out of a total of 244, for a success rate of 33%⁵⁰. When another algorithm (typically Rosetta) was combined with FoldX, the total success rate climbed to 47%. However, for each individual study, combined FoldX+Rosetta success rates varied between 14% and 68%, suggesting other factors are involved, such as the $\Delta\Delta G$ cutoff employed, or the quality of the input structure. When benchmarked against our experimental data, FoldX performed very poorly regardless of the value of the $\Delta\Delta G$ cutoff, but especially in the top 30 predicted variants (0% $E(N)$). In contrast, Rosetta FullMin achieved $\%E(N)$ values of roughly 20% over the top 30 variants, and PoPMuSiC+Rosetta NoMin maintained values above 30% for the majority of the cutoffs tested (Supplementary Fig. 4). These results clearly demonstrate that combinations of algorithms can improve the outcome of $\Delta\Delta G$ cutoff stability studies.

Comparing with deep mutational scanning studies. By coupling high-throughput functional selections with next generation sequencing, DMS can provide mutational data on thousands or even millions of variants with relatively little experimental effort^{26,27}. This technology is being applied to an increasing number of proteins and has the

potential to supply a wealth of new data to train stability prediction tools⁵¹, provided the DMS technique can be properly validated. Serendipitously, a DMS study was performed on every single mutant and nearly every double-mutant of G β 1⁵², allowing for a direct comparison with the thermodynamic stability data presented here. Using a selection based on binding to IgG Fc, Olson et al. found that fitness values obtained using binding affinity enrichment ($\ln W$) correlated very poorly ($r = 0.013$) with $\Delta\Delta G$ values reported in the literature for 82 single mutants ($\Delta\Delta G_{lit}$). When we compared $\ln W$ with the $\Delta\Delta G$ values from our larger set of 830 single mutants, we found a better, but still small correlation ($r = 0.19$) (Supplementary Fig. 5a).

To address this issue, Olson et al. devised a strategy to estimate single mutant stabilities from their DMS fitness data. This approach requires identifying destabilized mutational backgrounds using double mutant fitness data so that the functional effect of a second mutation in these backgrounds could be used to compute single mutant $\Delta\Delta G$ s. They identified five background mutations that produced a large correlation ($r = 0.91$) with $\Delta\Delta G_{lit}$ and later demonstrated an approach (see Wu et al.⁵³) that avoids the need for pre-existing stability data. In Fig. 7a, we plot our experimental $\Delta\Delta G$ s vs. those predicted using the Wu et al. method ($\Delta\Delta G_{Wu}$) for 794 single mutants. The correlation ($r = 0.60$) is significantly lower than the value obtained using the smaller $\Delta\Delta G_{lit}$ dataset ($r = 0.91$). A closer look at the 82 mutants in $\Delta\Delta G_{lit}$ reveals a relatively small % of mutations in the core and a bias towards Ala substitutions, resulting in a dataset that does not reflect the breadth of possible mutations in the entire domain (Table 1). As seen in Supplementary Fig. 5b, the limited number of mutants in $\Delta\Delta G_{lit}$ masks the

lower correlation between $\Delta\Delta G$ and $\Delta\Delta G_{\text{Wu}}$ by serendipitously avoiding off-diagonal single mutants.

A recent report by Otwinowski reanalyzed the Olson et al. fitness data with a method based on a thermodynamic model describing three states (bound-folded, unbound-folded, and unfolded) that avoids the need for preexisting mutational or structural data⁵⁴. The method calculates distinct energies for folding (E_{folding}) and binding (E_{binding}). We compare the E_{folding} energy ($\Delta\Delta G_{\text{Otwinowski}}$) with our experimental $\Delta\Delta G$ values in Fig. 7b, which shows an improved correlation ($r = 0.72$) over the Wu et al. method ($r = 0.60$). Supplementary Table 3 analyzes the correlations for the two methods by residue class, volume change, and polarity change. The $\Delta\Delta G_{\text{Otwinowski}}$ energy yields better correlations across the board, with the core continuing to show a significantly lower correlation. Thus, although DMS fitness data are poorly correlated with thermodynamic stability, simple biophysical models can be constructed that lead to significantly improved correlations. We expect that large, comprehensive datasets containing thermodynamic measurements such as those provided here will facilitate the development of improved methods to extract biophysical quantities (e.g., stability and binding) from fitness data, thus greatly expanding the utility of DMS and other deep sequencing techniques.

Discussion

We described an automated chemical denaturation methodology that produces high quality thermodynamic stability data at a throughput that enables the near total site-saturation mutagenesis of small protein domains. Although other low-cost methods such as thermal challenge assays or differential scanning fluorimetry can also provide useful

data, and deep sequencing approaches such as DMS can streamline the entire process, these methods do not directly report thermodynamic information. The automated pipeline described here makes gathering accurate thermodynamic stability data at a large scale feasible. The broad, unbiased nature of our near complete G β 1 single mutant study provides an important dataset for examining previously reported trends, evaluating stability prediction tools, and validating methods to extract stability values from DMS results.

We found that while the stability distribution of our G β 1 dataset features a long tail of destabilizing variants, most mutations (68%) are neutral. However, if variants without quantitative data and those omitted for technical reasons are assigned negative outcomes, destabilizing variants make up 45% of the 1,064 possible single mutants of G β 1, approaching predicted published values³¹. Other trends followed conventions, with mutations to Gly, Pro, and core positions almost always being deleterious. However, not all core positions show the same degree of sensitivity, as measures of residue burial such as C β atom depth and OSP were found to best correlate with median $\Delta\Delta G$ at each position. Although the correlation of residue burial with individual $\Delta\Delta G$ measurements was previously reported for a collection of variants across many proteins³⁶, our domain-wide dataset allows the position-specific nature of the relationship to be fully observed. Similarly, using our unique dataset to calculate median $\Delta\Delta G$ by incorporated amino acid reveals an unexpected tolerance for large hydrophobic amino acids. This preference extended across tertiary structure, and stability predictions on four other proteins confirmed this trend.

Evaluating three stability prediction algorithms against our dataset, we found that all performed moderately and recapitulated the general trends of the data. The flexible backbone Rosetta method (SomeMin) provided the best overall Pearson correlation ($r = 0.64$), but all of the Rosetta methods and PoPMuSiC performed equally by the Spearman rank correlation coefficient. Except for PoPMuSiC, all methods showed higher correlations in the boundary than on the surface ($r = \sim 0.7$ and ~ 0.5 , respectively), all showed consistently lower correlations for mutations at core positions ($r = 0.13$ to 0.37), and nearly all were better at predicting large to small mutations than small to large ones.

Overall, the Rosetta SomeMin method was the most accurate stability algorithm tested here. It gives the best Pearson correlation for nearly every mutational category and is near the top in non-parametric methods as well. However, Rosetta SomeMin, and to a greater extent, Rosetta FullMin, require the most computational resources. For lower computational cost, PoPMuSiC provides the next best correlation coefficients on our quantitative dataset. For identification of the most stable single mutants, the combination of PoPMuSiC and Rosetta NoMin gave the best overall performance in each of the metrics tested. Both methods are computationally efficient, and when combined give enrichment values over 30% and *PPVs* over 90% after analyzing the predicted top 100 variants.

DMS holds great promise as an extremely high-throughput method for obtaining mutational data for entire protein domains. However, correlating the fitness data to thermodynamic quantities such as stability is not straightforward, given that the selection method provides only an indirect measure of stability. In comparing our $\Delta\Delta G$

values against strategies designed to extract stabilities from high-throughput fitness data, we find that a simple thermodynamic model that distinguishes binding and folding energies results in a Pearson correlation coefficient of $r = 0.7$. Even higher correlations are achieved by omitting core variants, and this strategy could yield useful training sets in the near term.

Beyond the engineering insights described here, it is our hope that our single mutant dataset of thermodynamic stabilities will prove to be a powerful training set for use in developing better stability prediction tools and better methods for deriving stabilities from high-throughput fitness data.

Methods

Liquid handling robotics. A 2-meter Freedom EVO (Tecan) liquid-handling robot was used to automate the majority of the experimental pipeline. The instrument includes an eight-channel fixed-tip liquid-handling arm, a 96 disposable-tip single-channel liquid-handling arm, and a robotic plate-gripping arm. The robot's deck features a fast-wash module, a refrigerated microplate carrier, a microplate orbital shaker, a SPE vacuum system, an integrated PTC-200 PCR machine (Bio-Rad Laboratories), stacks and hotels for microplates, and an integrated Infinite M1000 fluorescence microplate reader (Tecan). All molecular biology methods were developed *de novo* and optimized as necessary.

Site-directed mutagenesis. The G β 1 gene, with an N-terminal hexahistidine tag, was inserted into pET11a under control of an IPTG inducible T7 promoter. Mutagenic oligonucleotides were ordered from Integrated DNA Technologies in a 96-well format

(150 μ M concentration, 25 nmole scale) and purified by standard desalting. The site-directed mutagenesis reaction was performed in two parts: (1) diluted mutagenic oligonucleotides were mixed with a master mix solution composed of Hot-start Phusion DNA polymerase (NEB), GC Phusion buffer, dNTPs, the plasmid template, and the non-mutagenic flanking oligonucleotide, followed by (2) mixing $\frac{1}{4}$ of the first step product with a similar master mix solution that omits the flanking oligonucleotide. The PCR cycling conditions for the two parts were: (1) a 30 s preincubation at 98°C followed by 15 thermocycling steps (98°C, 8 s; 62°C, 15 s; 72°C, 20 s), and (2) a 30 s preincubation at 98°C followed by 25 thermocycling steps (98°C, 8 s; 72°C, 3 min) followed by a final extension step at 72°C for 5 min. After mutagenesis, samples were mixed into an 8%-by-volume Dpn1 (NEB) digestion reaction (37°C, 1 h) to remove the parental template plasmid.

During development, reactions were diagnosed by E-Gel 96 (Invitrogen) electrophoresis systems, with loading performed by the liquid-handling robot. Visualization of the desired first-step and second-step products would guarantee positive mutagenesis. Almost 85% of all site-directed mutagenesis reactions were successful in the first pass.

Bacterial manipulation and sequence verification. Dpn1 digested products were mixed with homemade chemically competent BL21 Gold DE3 cells⁵⁵ in a 20 μ L total reaction volume, and incubated at 4°C for 10 min. After heat shock (42°C, 45 s) on the PCR machine, the bacterial transformations were recovered by adding 100 μ L of SOC media, and shaken off robot at 1200 rpm for 1 h at 37°C on a microplate shaker (Heidolph).

The transformation mixtures were plated by the liquid-handling robot onto 48-well LB agar Qtrays (Genetix) and spread by sterile beads⁵⁵. The Qtrays were incubated off robot for 14 h at 37°C. For each mutagenesis reaction, eight colonies were picked by a colony-picking robot (Qbot, Genetix) into 384-well plates (Genetix) filled with LB/10% glycerol. The 384-well receiving plates were incubated overnight at 37°C, after which 2 of the 8 cultures per mutagenesis reaction were used to inoculate 96-well microplates containing LB/10% glycerol. These 96-well glycerol stock plates were grown overnight at 37°C, replicated, and sent to Beckman Genomics for sequencing.

After analyzing the sequencing data, missing library members could be recovered either by sending more picked colonies from the 384-well receiving plate, or by redoing the mutagenesis reaction with different PCR conditions. Once all of the mutants were constructed, work lists were generated for the liquid-handling robot to cherry-pick from the replicated 96-well glycerol stock plates and inoculate into 96-well master stock plates containing LB/10% glycerol. The master stock plates were then incubated overnight at 37°C and frozen at -80°C until needed.

Protein expression and purification. Small volumes from replicated master stock plates were used to inoculate 5 mL of Instant TB auto-induction media (Novagen) in 24-well round-bottom plates (Whatman). The 24-well plates were incubated overnight, shaking at 250 rpm, at 37°C. The expression cultures were then pelleted, lysed with a sodium phosphate lysis buffer solution (pH 8) containing CellLytic B (Sigma Aldrich), lysozyme, and HC benzonase (Sigma Aldrich). Lysates were then added directly to 96-well His-Select Ni-NTA resin filter plates (Sigma Aldrich) and processed off-robot by centrifugation. His-tagged protein was washed and eluted in sodium phosphate buffer

(pH 8) containing 0 mM and 100 mM imidazole, respectively. Protein samples were diluted five-fold into sodium phosphate buffer (pH 6.5), thereby diluting the final amount of imidazole in each sample before stability determination.

Plate-based stability assay. Large volumes (0.2 L) of each concentration of a 24-point gradient of GdmCl in sodium phosphate buffer (pH 6.5) were constructed using graduated cylinders and dispensed into 96-well deep-well plates by a multi-channel pipettor. These reagent reservoirs, along with the liquid-handling robot, greatly simplified and sped up the stability assay previously described²². Each stability assay was comprised of 24 individual solutions containing 1 part purified protein to 4 parts GdmCl/buffer solution, and measured by the integrated plate reader for Trp fluorescence (Ex: 295 nm, Em: 341 nm). The assay employed 384-well UV-Star plates (Greiner) that allowed 16 different protein mutants to be measured per plate, thus requiring 6 of these plates per 96-well master stock plate. All variants were measured 2–6 times. Data were analyzed as described previously²².

Positional sensitivity. Positional sensitivity was evaluated via two metrics: (1) the median $\Delta\Delta G$ value and (2) sequence entropy. The median $\Delta\Delta G$ value for each position (j) was calculated by finding the median of $\Delta\Delta G$ values for all mutations measured at j , where mutations in the qualitative dataset were assigned a $\Delta\Delta G$ value of -4 kcal/mol.

The sequence entropy at a position j was calculated as $s^{(j)} = -\sum_{i=1}^{20} p_i^{(j)} \ln p_i^{(j)}$ where $p_i^{(j)}$, the probability of a given amino acid i at position j was determined by $p_i =$

$e^{\Delta\Delta G_i/kT} / \sum_{i=1}^{20} e^{\Delta\Delta G_i/kT}$. The WT residue was assigned a $\Delta\Delta G$ value of zero and mutations

in the qualitative dataset were assigned a value of -4 kcal/mol. The positional sensitivity

at each position was visualized on the crystal structure of G β 1 (PDB ID: 1PGA) using VMD⁵⁶.

Protein attributes. All structure-based attributes were calculated using the crystal structure of G β 1 (PDB ID: 1PGA). Occluded surface packing³⁹ was calculated using software downloaded from <http://pages.jh.edu/pfleming/sw/os/>. Root mean square fluctuation (RMSF) was calculated over a 20 ns molecular dynamics trajectory in full solvent using NAMD⁵⁷. The depth of the C β atom was calculated by the RESCLASS algorithm⁴ to decide core, boundary, and surface residues. Linear regression with 10-fold cross validation was performed with scikit-learn⁵⁸ to identify attributes that correlate highly with positional sensitivity. Recursive feature elimination was also performed with scikit-learn using a ridge estimator, and 5-fold cross validation was performed to evaluate combinations of attributes. Recursive feature elimination was also performed with scikit-learn to evaluate combinations of attributes.

Stability prediction algorithms. The crystal structure of G β 1 (PDB ID: 1PGA) was used as the input structure for all algorithms. The webserver for PoPMuSiC version 3, located at <http://www.dezyme.com>, was used to perform a “Systematic” command on the G β 1 crystal structure. A copy of FoldX (version 3.0, beta 5) was retrieved from <http://foldx.crg.es>. The crystal structure was prepared by using the “RepairPDB” command to perform Asn, Gln, and His flips, alleviate small van der Waals clashes, and optimize WT rotamer packing. Every mutant in the dataset was constructed through the “BuildModel” command, and the difference in energy between the WT reference and the corresponding mutant was averaged over five trials. A copy of Rosetta (version 3.3) was

retrieved from <http://www.rosettacommons.org>. The ddg_monomer application was used to generate single mutant stability data from the G β 1 crystal structure. We followed the available online documentation in order to prepare all necessary input files. Option sets described in the documentation pertain to the various Rosetta iterations tested in this paper (NoMin: low-resolution protocol; SomeMin: high-resolution protocol; FullMin: high-resolution protocol with an empty distance restraints file).

Statistical visualization and analysis. All plots were generated using the software Tableau (Seattle, WA). Custom python scripts were developed to calculate the large number of thermodynamic stability curve fits. Correlation coefficients (Pearson's and Spearman's) were calculated either in Tableau or in the software package R (version 3.2.2). The ROCR package for R was used for classification and receiver operator characteristic analysis⁵⁹.

Data availability. The $\Delta\Delta G$ distribution of G β 1 single mutants generated during this work is publicly available in ProtaBank (<https://protabank.org>), a protein engineering data repository, under the ID gwoS2haU3. All of the other data that support the conclusions of the study are available from A.N. upon request.

References

1. Bommarius, A.S. & Paye, M.F. Stabilizing biocatalysts. *Chem. Soc. Rev.* **42**, 6534-6565 (2013).
2. Goldenzweig, A. & Fleishman, S. Principles of protein stability and their application in computational design. *Annu. Rev. Biochem.* **87**(2018).
3. Rouet, R., Lowe, D. & Christ, D. Stability engineering of the human antibody repertoire. *FEBS Lett.* **588**, 269-277 (2014).
4. Dahiyat, B.I. & Mayo, S.L. De novo protein design: fully automated sequence selection. *Science* **278**, 82-87 (1997).
5. Das, R. & Baker, D. Macromolecular modeling with Rosetta. *Annu. Rev. Biochem.* **77**, 363-382 (2008).
6. Dehouck, Y., Grosfils, A., Folch, B., Gilis, D., Bogaerts, P. & Rooman, M. Fast and accurate predictions of protein stability changes upon mutations using statistical potentials and neural networks: PoPMuSiC-2.0. *Bioinformatics* **25**, 2537-2543 (2009).
7. Guerois, R., Nielsen, J.E. & Serrano, L. Predicting changes in the stability of proteins and protein complexes: a study of more than 1000 mutations. *J. Mol. Biol.* **320**, 369-387 (2002).
8. Kellogg, E.H., Leaver-Fay, A. & Baker, D. Role of conformational sampling in computing mutation-induced changes in protein structure and stability. *Proteins* **79**, 830-838 (2011).
9. Malakauskas, S.M. & Mayo, S.L. Design, structure and stability of a hyperthermophilic protein variant. *Nat Struct Biol* **5**, 470-475 (1998).

10. Pires, D.E.V., Chen, J., Blundell, T.L. & Ascher, D.B. In silico functional dissection of saturation mutagenesis: Interpreting the relationship between phenotypes and changes in protein stability, interactions and activity. *Sci. Rep.* **6**, 19848 (2016).
11. Burgess, D.J. Disease genetics: network effects of disease mutations. *Nat. Rev. Genet.* **16**, 317 (2015).
12. Potapov, V., Cohen, M. & Schreiber, G. Assessing computational methods for predicting protein stability upon mutation: good on average but not in the details. *Protein Eng. Des. Sel.* **22**, 553-560 (2009).
13. Khan, S. & Vihinen, M. Performance of protein stability predictors. *Hum. Mutat.* **31**, 675-684 (2010).
14. Davey, J.A. & Chica, R.A. Optimization of rotamers prior to template minimization improves stability predictions made by computational protein design. *Protein Sci.* **24**, 545-560 (2015).
15. Alber, T. Mutational effects on protein stability. *Annu. Rev. Biochem.* **58**, 765-798 (1989).
16. Bowie, J.U., Reidhaar-Olson, J.F., Lim, W.A. & Sauer, R.T. Deciphering the message in protein sequences: tolerance to amino acid substitutions. *Science* **247**, 1306-1310 (1990).
17. Matthews, B.W. Structural and genetic analysis of protein stability. *Annu. Rev. Biochem.* **62**, 139-160 (1993).
18. Fersht, A.R. & Serrano, L. Principles of protein stability derived from protein engineering experiments. *Curr. Opin. Struct. Biol.* **3**, 75-83 (1993).

19. Kumar, M.D.S., Bava, K.A., Gromiha, M.M., Prabakaran, P., Kitajima, K., Uedaira, H. et al. ProTherm and ProNIT: thermodynamic databases for proteins and protein-nucleic acid interactions. *Nucleic Acids Res.* **34**, D204-206 (2006).
20. Wang, C.Y., Chang, P.M., Ary, M.L., Allen, B.D., Chica, R.A., Mayo, S.L. et al. ProtaBank: A repository for protein design and engineering data. *Protein Sci.* **27**, 1113-1124 (2018).
21. Markiewicz, P., Kleina, L.G., Cruz, C., Ehret, S. & Miller, J.H. Genetic studies of the lac repressor. XIV. Analysis of 4000 altered Escherichia coli lac repressors reveals essential and non-essential residues, as well as "spacers" which do not require a specific sequence. *J. Mol. Biol.* **240**, 421-433 (1994).
22. Allen, B.D., Nisthal, A. & Mayo, S.L. Experimental library screening demonstrates the successful application of computational protein design to large structural ensembles. *Proc. Natl. Acad. Sci. USA* **107**, 19838-19843 (2010).
23. Aucamp, J.P., Cosme, A.M., Lye, G.J. & Dalby, P.A. High-throughput measurement of protein stability in microtiter plates. *Biotechnol Bioeng* **89**, 599-607 (2005).
24. Lavinder, J.J., Hari, S.B., Sullivan, B.J. & Magliery, T.J. High-throughput thermal scanning: a general, rapid dye-binding thermal shift screen for protein engineering. *J Am Chem Soc* **131**, 3794-3795 (2009).
25. Rocklin, G.J., Chidyausiku, T.M., Goresnik, I., Ford, A., Houliston, S., Lemak, A. et al. Global analysis of protein folding using massively parallel design, synthesis, and testing. *Science* **357**, 168-175 (2017).

26. Araya, C.L. & Fowler, D.M. Deep mutational scanning: assessing protein function on a massive scale. *Trends Biotechnol.* **29**, 435-442 (2011).
27. Fowler, D.M. & Fields, S. Deep mutational scanning: a new style of protein science. *Nat. Methods* **11**, 801-807 (2014).
28. Myers, J.K., Pace, C.N. & Scholtz, J.M. Denaturant m values and heat capacity changes: relation to changes in accessible surface areas of protein unfolding. *Protein Sci.* **4**, 2138-2148 (1995).
29. Pace, C.N. Determination and analysis of urea and guanidine hydrochloride denaturation curves. *Methods Enzymol.* **131**, 266-280 (1986).
30. Santoro, M.M. & Bolen, D.W. Unfolding free energy changes determined by the linear extrapolation method. 1. Unfolding of phenylmethanesulfonyl alpha-chymotrypsin using different denaturants. *Biochemistry* **27**, 8063-8068 (1988).
31. Tokuriki, N., Stricher, F., Schymkowitz, J., Serrano, L. & Tawfik, D.S. The stability effects of protein mutations appear to be universally distributed. *J. Mol. Biol.* **369**, 1318-1332 (2007).
32. Tokuriki, N. & Tawfik, D.S. Stability effects of mutations and protein evolvability. *Curr. Opin. Struct. Biol.* **19**, 596-604 (2009).
33. Henikoff, S. & Henikoff, J.G. Amino acid substitution matrices from protein blocks. *Proc. Natl. Acad. Sci. USA* **89**, 10915-10919 (1992).
34. Huang, W., Petrosino, J., Hirsch, M., Shenkin, P.S. & Palzkill, T. Amino acid sequence determinants of beta-lactamase structure and activity. *J. Mol. Biol.* **258**, 688-703 (1996).

35. Rennell, D., Bouvier, S.E., Hardy, L.W. & Poteete, A.R. Systematic mutation of bacteriophage T4 lysozyme. *J. Mol. Biol.* **222**, 67-88 (1991).
36. Chakravarty, S. & Varadarajan, R. Residue depth: a novel parameter for the analysis of protein structure and stability. *Structure* **7**, 723-732 (1999).
37. Tan, K.P., Nguyen, T.B., Patel, S., Varadarajan, R. & Madhusudhan, M.S. Depth: a web server to compute depth, cavity sizes, detect potential small-molecule ligand-binding cavities and predict the pKa of ionizable residues in proteins. *Nucleic Acids Res.* **41**, W314-321 (2013).
38. Pattabiraman, N., Ward, K.B. & Fleming, P.J. Occluded molecular surface: analysis of protein packing. *J. Mol. Recognit.* **8**, 334-344 (1995).
39. Fleming, P.J. & Richards, F.M. Protein packing: dependence on protein size, secondary structure and amino acid composition. *J. Mol. Biol.* **299**, 487-498 (2000).
40. Valdar, W.S.J. Scoring residue conservation. *Proteins* **48**, 227-241 (2002).
41. Kyte, J. & Doolittle, R.F. A simple method for displaying the hydrophobic character of a protein. *J. Mol. Biol.* **157**, 105-132 (1982).
42. Dixon, D.A. & Lipscomb, W.N. Electronic structure and bonding of the amino acids containing first row atoms. *J. Biol. Chem.* **251**, 5992-6000 (1976).
43. Dehouck, Y., Kwasigroch, J.M., Gilis, D. & Rooman, M. PoPMuSiC 2.1: a web server for the estimation of protein stability changes upon mutation and sequence optimality. *BMC Bioinformatics* **12**, 151 (2011).
44. Ayuso-Tejedor, S., Abián, O. & Sancho, J. Underexposed polar residues and protein stabilization. *Protein Eng. Des. Sel.* **24**, 171-177 (2011).

45. Broom, A., Jacobi, Z., Trainor, K. & Meiering, E.M. Computational tools help improve protein stability but with a solubility tradeoff. *J. Biol. Chem.* **292**, 14349-14361 (2017).
46. Cordes, M.H. & Sauer, R.T. Tolerance of a protein to multiple polar-to-hydrophobic surface substitutions. *Protein Sci.* **8**, 318-325 (1999).
47. Machius, M., Declerck, N., Huber, R. & Wiegand, G. Kinetic stabilization of *Bacillus licheniformis* alpha-amylase through introduction of hydrophobic residues at the surface. *J. Biol. Chem.* **278**, 11546-11553 (2003).
48. Poso, D., Sessions, R.B., Lorch, M. & Clarke, A.R. Progressive stabilization of intermediate and transition states in protein folding reactions by introducing surface hydrophobic residues. *J. Biol. Chem.* **275**, 35723-35726 (2000).
49. Baase, W.A., Liu, L., Tronrud, D.E. & Matthews, B.W. Lessons from the lysozyme of phage T4. *Protein Sci.* **19**, 631-641 (2010).
50. Buß, O., Rudat, J. & Ochsenreither, K. FoldX as protein engineering tool: better than random based approaches? *Comput Struct Biotechnol J* **16**, 25-33 (2018).
51. Araya, C.L. & Fowler, D.M. Deep mutational scanning: assessing protein function on a massive scale. *Trends Biotechnol* **29**, 435-442 (2011).
52. Olson, C.A., Wu, N.C. & Sun, R. A comprehensive biophysical description of pairwise epistasis throughout an entire protein domain. *Curr. Biol.* **24**, 2643-2651 (2014).
53. Wu, N.C., Olson, C.A. & Sun, R. High-throughput identification of protein mutant stability computed from a double mutant fitness landscape. *Protein Sci.* **25**, 530-539 (2015).

54. Otwinowski, J. Biophysical inference of epistasis and the effects of mutations on protein stability and function. *arXiv*, 1-18 (2018).
55. Klock, H.E. & Lesley, S.A. The Polymerase Incomplete Primer Extension (PIPE) method applied to high-throughput cloning and site-directed mutagenesis. *Methods Mol. Biol.* **498**, 91-103 (2009).
56. Humphrey, W., Dalke, A. & Schulten, K. VMD: visual molecular dynamics. *J Mol Graph* **14**, 33-38 (1996).
57. Phillips, J.C., Braun, R., Wang, W., Gumbart, J., Tajkhorshid, E., Villa, E. et al. Scalable molecular dynamics with NAMD. *J Comput Chem* **26**, 1781-1802 (2005).
58. Pedregosa, F., Varoquaux, G., Gramfort, A., Michel, V. & Thirion, B. Scikit-learn: Machine learning in Python. *JMLR* **12**, 2825-2830 (2011).
59. Sing, T., Sander, O., Beerenwinkel, N. & Lengauer, T. ROCR: visualizing classifier performance in R. *Bioinformatics* **21**, 3940-3941 (2005).
60. Kabsch, W. & Sander, C. Dictionary of protein secondary structure: pattern recognition of hydrogen-bonded and geometrical features. *Biopolymers* **22**, 2577-2637 (1983).

Acknowledgements

A.N. thanks Jost Vielmetter for advice and feedback on the automated platform. S.L.M. acknowledges grants from the National Security Science and Engineering Faculty Fellowship program and the Defense Advanced Research Projects Agency Protein Design Processes program.

Author contributions

A.N. and S.L.M designed the research. A.N. developed the experimental approach, performed all experiments, and managed the data. A.N., C.Y.W., and M.L.A. analyzed the data and wrote the paper with input from S.L.M.

Additional information

Competing interests: The authors declare no competing interests.

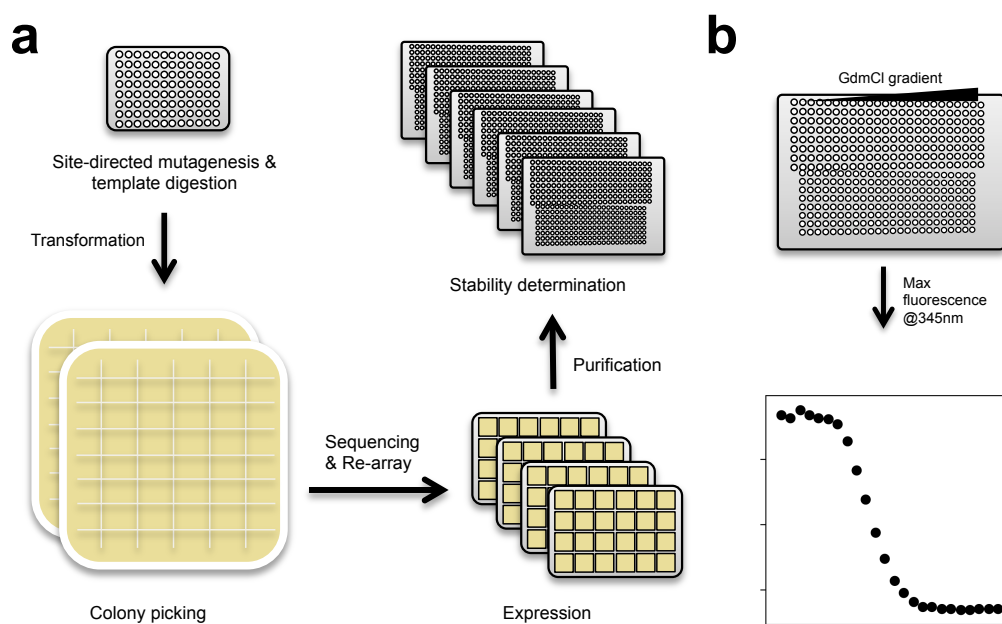


Fig. 1 Automated site-directed mutagenesis and stability determination pipeline. **a** Modular protocols enable the rapid construction, sequence verification, and stability determination of single mutant variants. For illustrative purposes, each step shows the number of plates required for 96 individual reactions. Oligonucleotides direct mutagenesis reactions on 96-well PCR plates followed by bacterial transformation and plating onto 48-well agar trays. Individual colonies are picked, cultured, and re-arrayed after successful sequence validation. Confirmed variants are expressed in 24-well culture blocks and NiNTA purified. Each reaction was tracked via a database throughout the pipeline, allowing for method optimization. **b** Thermodynamic stability was determined by measuring Trp fluorescence in response to a 24-point GdmCl gradient. Each row of a 384-well plate is one protein stability curve from which the concentration of denaturant at the midpoint of the unfolding transition (C_m) is directly measured. After estimating the slope of the curve (m -value), the change in the free energy of unfolding ($\Delta\Delta G$) of each variant relative to WT is calculated by taking the difference between the

WT and mutant C_m values and multiplying by their mean m -value (see Supplementary Methods and Supplementary Fig. 2).

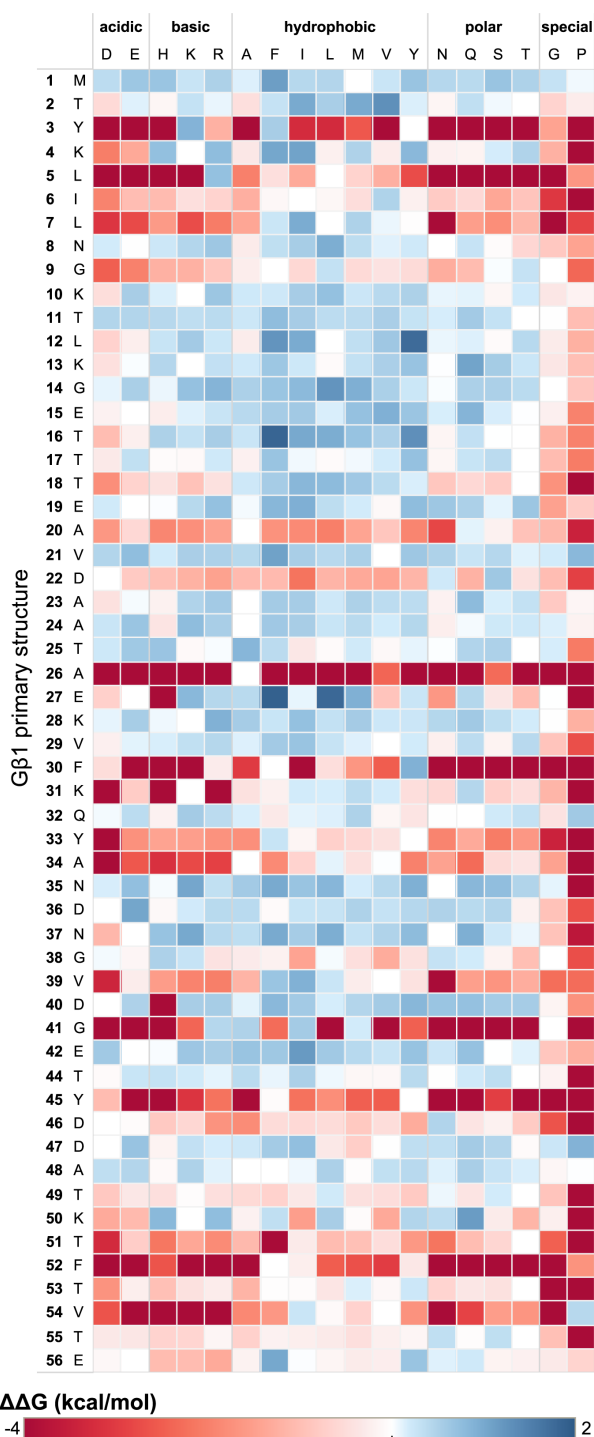


Fig. 2 Single mutant thermodynamic stability landscape of Gβ1. The vertical axis of the mutational matrix depicts the primary structure of Gβ1, with the position and WT amino acid as columns. The horizontal axis depicts mutant amino acids examined in the study,

grouped by amino acid type. Variants are colored by their determined $\Delta\Delta G$ value where red is destabilizing, blue is stabilizing, and white is neutral. Self-identity mutations such as M1M have $\Delta\Delta G = 0$ and thus are colored white. Variants from the qualitative dataset are assigned an arbitrary value of -4 kcal/mol and are colored accordingly.

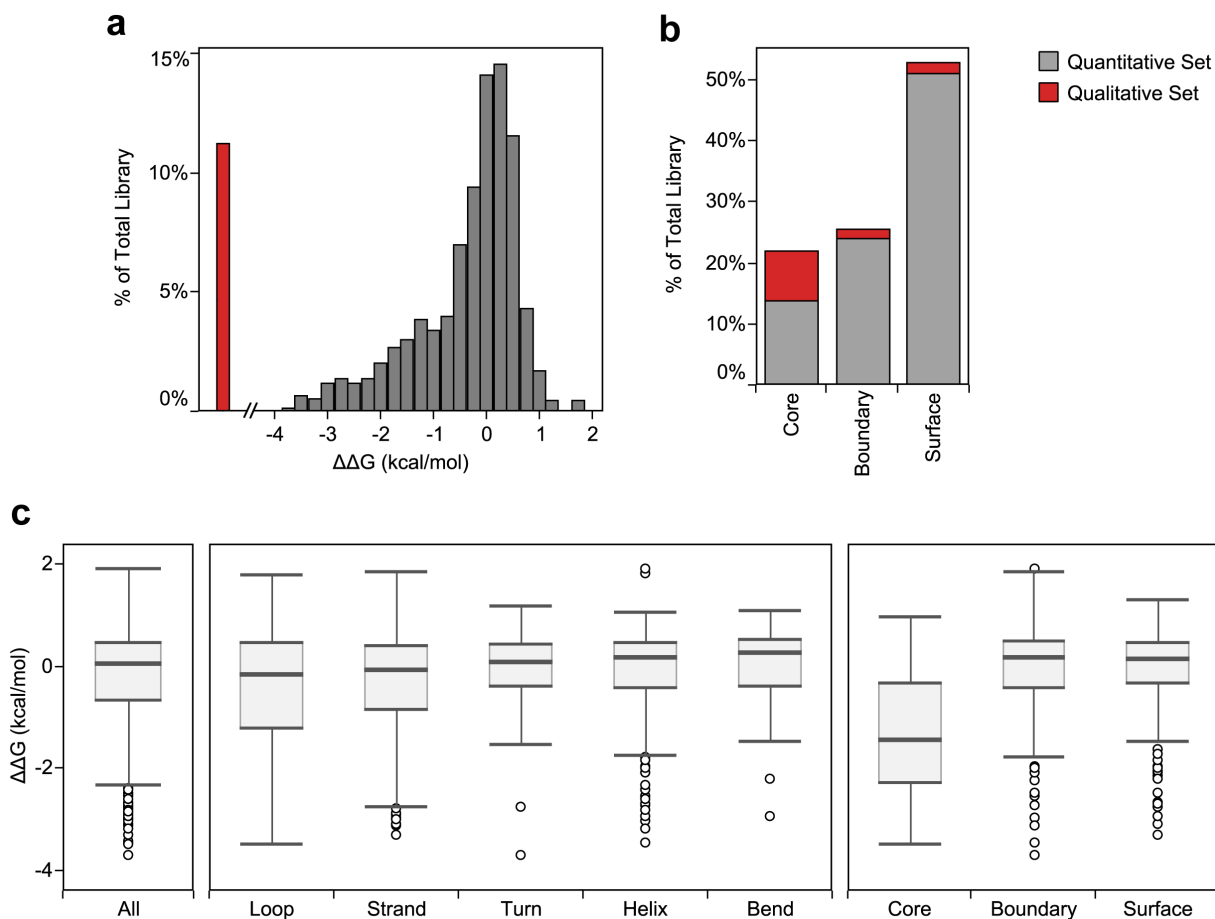


Fig. 3 Stability distribution of G β 1 single mutants. **a–b** The 935-member dataset is split between variants with quantitative data (gray) and those with only qualitative data (red) due to poor stability or misfolding. **a** The $\Delta\Delta G$ distribution is split into 0.25 kcal/mol bins. Variants belonging to the qualitative dataset are shown to the left of the distribution, indicating $\Delta\Delta G$ s < -4 kcal/mol. **b** Variants are binned into core, boundary, or surface using RESCLASS⁴. **c** Box and whisker plots of the quantitative dataset describe the median, the quartile cutoffs, and the outlier cutoffs of the $\Delta\Delta G$ distribution for all the residues (All), binned into secondary structure classifications as defined by DSSP⁶⁰, or binned by RESCLASS. Outliers are shown as unfilled circles and are defined as points

that are $1.5 \times$ interquartile range above or below the 3rd quartile or 1st quartile, respectively.

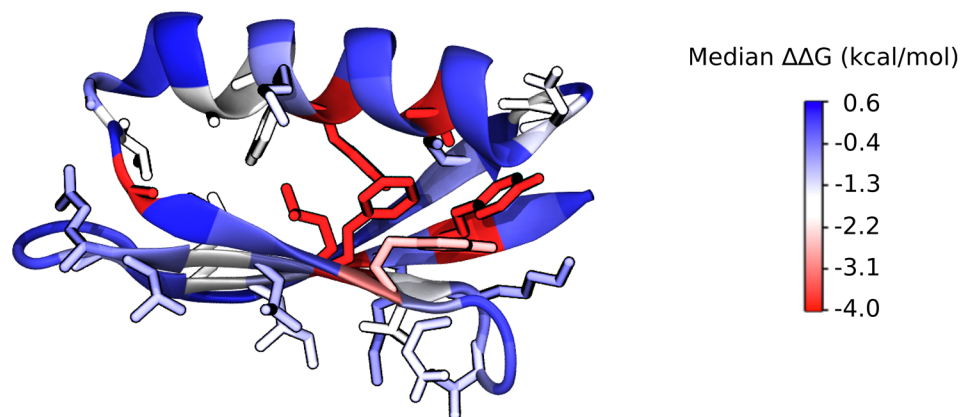


Fig. 4 Positional sensitivity (median $\Delta\Delta G$ at each position) of Gβ1. Gβ1 X-ray crystal structure (PDB ID: 1PGA) is colored by the positional sensitivity at each position. Sidechain atoms are shown for residues with a positional sensitivity score less than zero (destabilized).

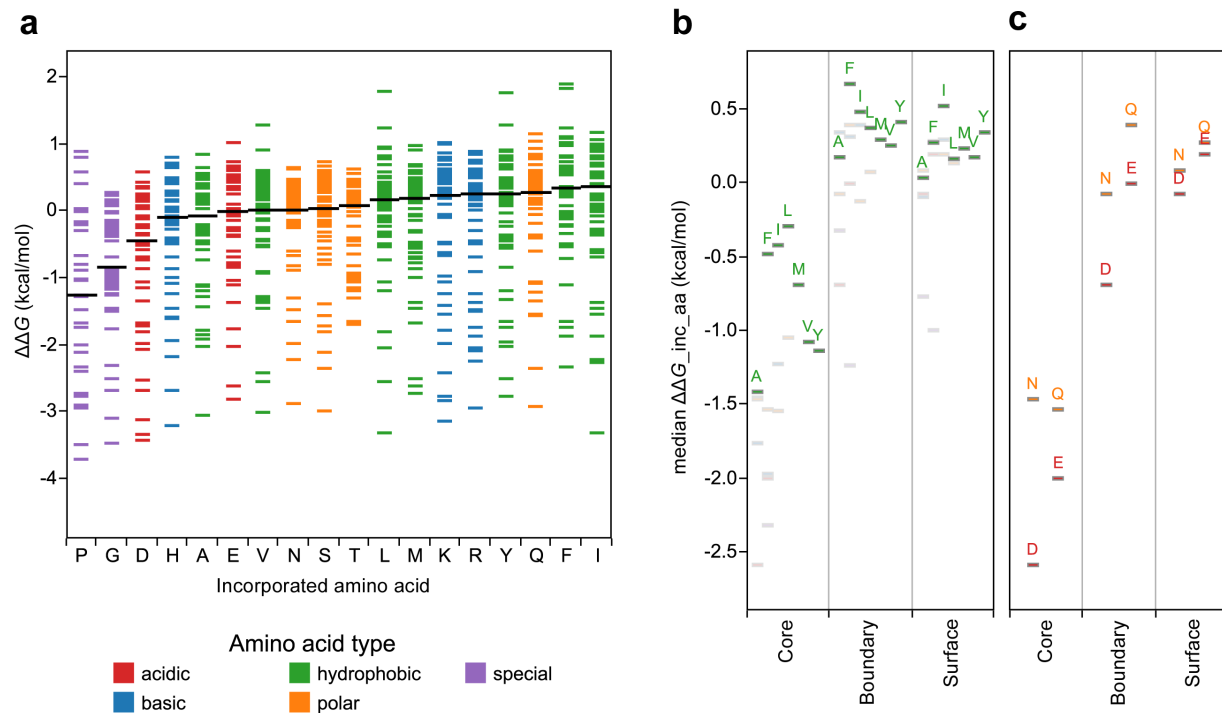


Fig. 5 $\Delta\Delta G$ distribution by incorporated amino acid. Amino acids are colored by physiochemical type. **a** Individual variants are shown as Gantt lines and distributed by the incorporated amino acid. The amino acid bins are ordered from left to right by the median $\Delta\Delta G$ of each distribution (black lines). **b** Median $\Delta\Delta G$ s of the incorporated amino acid distribution grouped by RESCLASS⁴. For clarity, only hydrophobic amino acids are labeled. **c** Median $\Delta\Delta G$ s of chemically similar pairs (D/E and N/Q), grouped by RESCLASS.

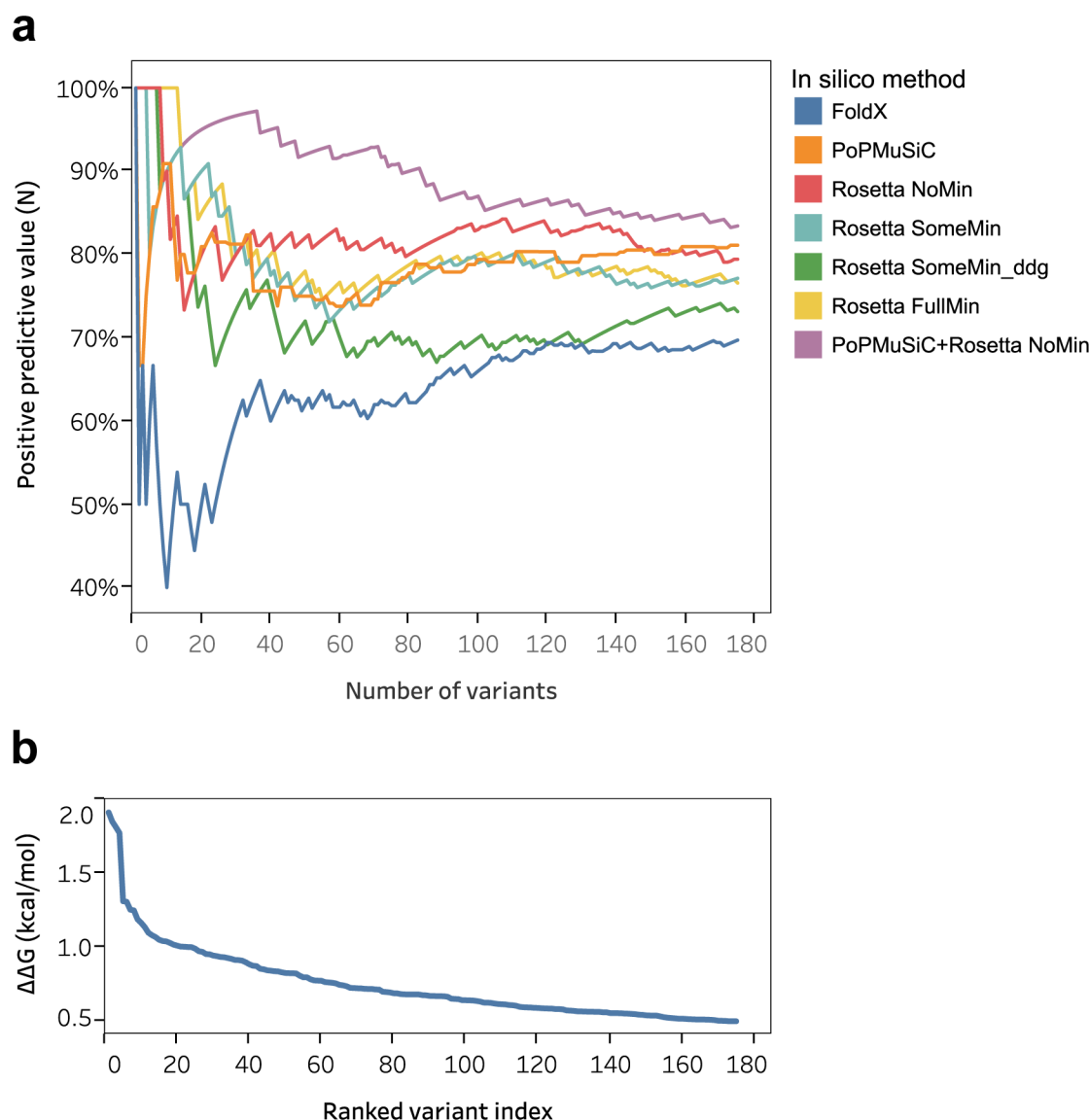


Fig. 6 Comparing stability prediction algorithms by positive predictive value, *PPV*. **a** *PPV(N)*, as defined in the text, is plotted as a function of the number of variants included in the list comparison. Only the top 175 G β 1 single mutants are shown, sorted by $\Delta\Delta G$. Each of the single algorithms and, for simplicity, only the best two-algorithm combination (PoPMuSiC+Rosetta NoMin) are shown, colored according to the legend. **b**

As a reference, experimental $\Delta\Delta G$ values are plotted as a function of the ranked variant index, a sorted list of the stability distribution.

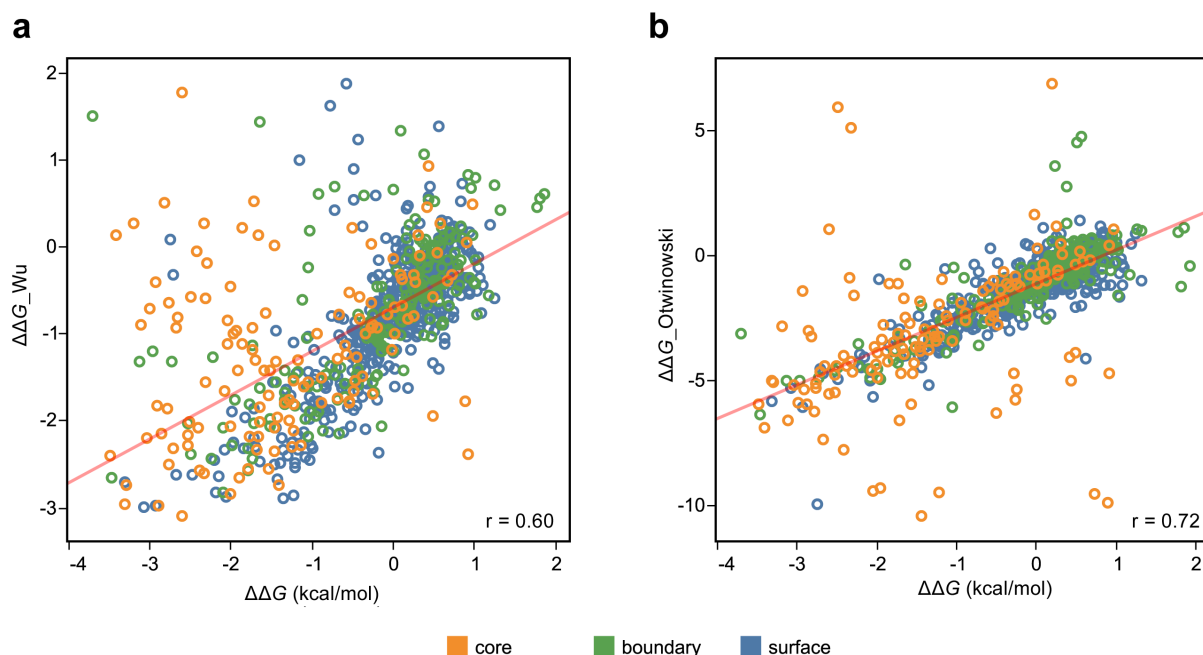


Fig. 7 Comparing experimental $\Delta\Delta G$ s with predictions obtained from DMS fitness data. G β 1 single mutant stabilities from our experimental quantitative dataset ($\Delta\Delta G$) are plotted against (a) $\Delta\Delta G$ values predicted from the DMS data using the Wu et al. method⁵³ ($\Delta\Delta G_{Wu}$) ($n = 794$) or (b) $E_{folding}$ values predicted from the DMS data using Otwinowski's three-state thermodynamic model⁵⁴ ($\Delta\Delta G_{Otwinowski}$) ($n = 812$). In both cases, DMS data is from Olson et al.⁵² Points are colored by RESCLASS⁴ values. A linear regression line is shown in red, and the correlation coefficient is shown in the lower right of each plot.

Table 1 Mutational composition of protein stability datasets

$\Delta\Delta G$ dataset	Total #	% surface	% boundary	% core	% +VolΔ	% -VolΔ	% Ala
FoldX training set ⁷	339	32	27	36	3	97	61
FoldX test set ⁷	625	32	30	35	5	95	54
PoPMuSiC training set ⁶	2644	26	32	40	33	67	28
PoPMuSiC test set ⁶	350	21	27	48	40	60	26
Rosetta test set ⁸	1210	32	30	38	16	84	47
$\Delta\Delta G_{lit}$ ⁵²	82	71	21	8	52	48	20
This dataset	935	53	25	22	56	44	5

Residues were classified as core, boundary or surface with the RESCLASS⁴ algorithm. Mutations with mislabeled or non-standard PDB data (< 5%) were omitted from residue classification. +Vol Δ , small to large mutations; -Vol Δ , large to small mutations.

Table 2 Algorithm performance by Pearson correlation

Algorithm	Backbone minimization ^a	Clash outliers ^b	Pearson correlation coefficient (<i>r</i>)					
			Overall	Surface ^c	Boundary ^c	Core ^c	+VolΔ	−VolΔ
PoPMuSiC		0	0.56	0.51	0.56	0.33	0.43	0.64
FoldX		17	0.51	0.42	0.68	0.17	0.46	0.56
Rosetta ^d								
NoMin	None	22	0.33	0.29	0.26	0.13	0.38	0.28
SomeMin	Constrained	17	0.64	0.53	0.73	0.37	0.56	0.66
SomeMin_ddg ^e	Constrained	6	0.54	0.49	0.68	0.15	0.46	0.66
FullMin	Unconstrained	3	0.60	0.52	0.69	0.24	0.48	0.69

Predicted $\Delta\Delta G$ s from stability algorithms were compared to experimental $\Delta\Delta G$ s for G β 1 single mutants in the quantitative dataset. Mutations with exceptionally high clash energies (clash outliers) were excluded when calculating each algorithm's correlation coefficient. +VolΔ, small to large mutations; −VolΔ, large to small mutations.

^a Level of backbone minimization after repacking for Rosetta methods.

^b Number of mutations with a calculated repulsive energy > 2 standard deviations above the mean.

^c Residues are classified as core, boundary, or surface using RESCLASS⁴.

^d Rosetta parameter sets NoMin, SomeMin, and FullMin were initially described as row 3, row 16, and row 19, respectively⁸.

^e Combines constrained backbone minimization with optimized reference energies trained on single mutant $\Delta\Delta G$ data from ProTherm.